Magnetocrystalline anisotropy and three-dimensional hopping conduction at the surface of $FeSb_2$

Jarryd A. Horn,[1] Yun Suk Eo,[1,2] Keenan Avers,[1] Hyeok Yoon,[1] Ryan G. Dorman,[1] Shanta R. Saha,[1] and Johnpierre Paglione[1,3]

[1]*Maryland Quantum Materials Center and Department of Physics, University of Maryland, College Park, Maryland 20742, USA*

[2]*Department of Physics, Texas Tech University, Lubbock, Texas 79409, USA*

[3]*Canadian Institute for Advanced Research, Toronto, Ontario, Canada M5G 1Z8*

(Received 5 September 2025; revised 22 December 2025; accepted 25 February 2026; published 24 March 2026)

Motivated by the recent discovery of metallic surface states in the *d*-electron Kondo insulator candidates FeSi and $FeSb_2$, along with some recent reports of magnetic correlations in the surface transport properties of FeSi, we have investigated the low-temperature surface magnetotransport properties of $FeSb_2$. By using a Corbino disk transport geometry, we were able to isolate the electrical transport properties of a single surface of our samples and study the [110] and [101] naturally forming faces separately. Studying the relationship between the applied magnetic field, current direction, and crystal symmetry has allowed us to separate possible contributions to the magnetotransport anisotropy. Unlike previous studies of SmB_6 surface states, we find no two-dimensional Drude-like dependence on field orientation relative to current direction, but instead a magnetocrystalline anisotropy that appears to originate from local moment scattering with a well-defined easy axis along the [100] direction. We compare these results with the magnetotransport properties of the conducting surface states on the [111] facet of FeSi. We also find evidence of three-dimensional variable-range-hopping conduction below the bulk-to-surface crossover, extending below 1 K, which implies that the electrical transport at the surface of these materials is carried by a thin but three-dimensional conducting channel, which is inconsistent with the lower dimensional states expected for a strong topological insulator.

DOI: 10.1103/5jfb-8p78

I. INTRODUCTION

Until recently, the study of Kondo insulator (KI) physics has been focused on materials with heavy *f*-electron orbitals near the Fermi level [1]. In typical KI systems, the local *f* moment hybridizes with conduction electrons to form a narrow gap, with well-studied examples being SmB_6 and YbB_{12} [2–7], and more recently $U_3Bi_4Ni_3$ [8]. In these particular systems, a clear plateau in the low-temperature electrical resistance is found to arise due to residual conduction from surface states that electrically short conduction from bulk activated charge carriers [9]. While angle-resolved photoemission spectroscopy (ARPES) and scanning tunneling microscopy quasiparticle interference studies on clean, *in situ* cleaved surfaces show evidence of these gapless surface states, the topological classification of these surface states is still heavily debated [10,11].

First reports of the Kondo insulator descriptions of FeSi and $FeSb_2$ came from examining the bulk magnetization of these materials and the apparent activation of a singlet ground state to a high-temperature paramagnetic state, consistent with singlet formation in Kondo insulators [12,13]. Speculation of topological Kondo insulator physics arose after the first reports of surface conduction in FeSi by dimensional scaling of resistance [14], followed by spectroscopic evidence of gapless surface states reported in $FeSb_2$ and FeSi by ARPES [15,16] and later demonstrated unambiguously by nonlocal transport [17]. Subsequent magnetoresistance (MR) measurements on FeSi showed that the surface states are magnetically correlated with evidence of magnetically ordered surface states [18–21]. Recent measurements of surface magnetotransport anisotropy in $FeSb_2$ suggest similarities between SmB_6 and $FeSb_2$ but do not report similar correlated physics as was found in FeSi [22], although theoretical calculations suggest that $FeSb_2$ is an incipient altermagnet which may stabilize order with doping [23].

The topological KI description of $FeSb_2$ is contested by spectroscopic and *ab initio* studies [24,25]. For example, Li *et al.* note that spectroscopic evidence supports the presence of surface states on the [010] and [110] surfaces with the absence of surface states on [001] surfaces of $FeSb_2$ [25]. The authors also propose an alternative theory to the Kondo insulator description of $FeSb_2$ involving an excitation of the bulk spin state across a multiplet gap. Another possible mechanism put forth by Chikina *et al.* and supported by *ab initio* calculations to match ARPES data is the possible existence of structural distortions at the surface, which would depend on how the surface is terminated [24].

In this paper, we report on low-temperature transport properties of the [110] and [101] surfaces of $FeSb_2$, demonstrating the crossover in magnetotransport anisotropy from the bulk-dominated conduction regime at high temperatures to the surface-dominated conduction regime at low temperatures by comparing the angle dependence of the MR. A detailed analysis of the magnetic field dependence of the low-temperature surface transport is shown to be consistent with local moment scattering, and comparisons to similar measurements on the [111] surface of FeSi indicate that magnetic correlations observed in the ferromagnetic surface states of FeSi may play a similar role on the surface of $FeSb_2$.

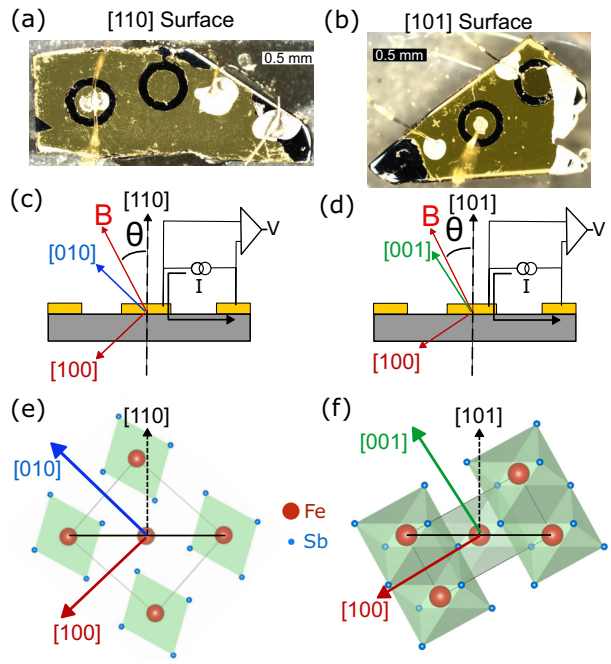

FIG. 1. (a), (b) $FeSb_2$ transport samples patterned with Corbino disk transport geometries deposited with Ti/Au (yellow) on the $FeSb_2$ (black) [110] surface and [101] surface. Silver pasted wire contacts are shown in white spots, through which current flows and across which voltage is measured as depicted in panels (c) and (d). (c), (d) Schematic of magnetic field rotation in and out of plane of the [110] surface *a*-*b* plane and [101] surface *a*-*c* plane, where yellow represents the Ti/Au layer and gray represents $FeSb_2$. (e), (f) Schematic of the *a*-*b* plane and *a*-*c* plane aligned with the orientation of panels (c) and (d).

II. EXPERIMENTAL DETAILS

While all other previously reported topological Kondo insulator candidates, including FeSi, have cubic crystal symmetry, $FeSb_2$ crystallizes with orthorhombic crystal symmetry [26] of space group *Pnnm* with unit cell dimensions of a=5.834 Å, b=6.530 Å, and c=3.193 Å. This complicates the study of surface states in this material, which entails a larger permutation space for surfaces and unique field directions. For this study, we will focus on the study of [110] and [101] surfaces because of the convenience of being provided with clean facets of these surfaces from crystal formation.

In order to carefully study the magnetotransport properties of the surface of $FeSb_2$, we obtained single-crystal samples with as-grown [110] and [101] facets. These samples were grown using molten antimony flux method (see, e.g., Ref. [27]), which provides large clean facets which are useful for patterning transport geometries, although it is important that we were sure to prepare samples free from Sb inclusions (see, e.g., Supplemental Material for our samples before Ti/Au deposition [28]). We pattern Corbino disks on those facets by standard photolithography followed by *e*-beam evaporation of Ti/Au (30A/1500A), as shown in Figs. 1(a) and 1(b). These metalized patterns not only confine the current path, but also provide excellent electrical contacts. This technique probes only a single surface and therefore provides a way to rotate the magnetic field in and out of the plane in which our current is confined [29]. When applied to a two-dimensional (2D) electron gas (2DEG), this method allows an accurate measurement of the 2D transport parameters, as has been shown with the surface states of SmB_6 [30]. The FeSi sample used in this paper is the same four-terminal [111] surface Corbino sample reported in previous reports [17,21].

This work is a follow-up to our previous work [17], in which we demonstrate that the bulk resistivity exceeds 10^6 Ω cm at the temperatures at which we perform these magnetotransport studies. Therefore, the transport contribution from the bulk can be estimated as a small dimensionless parameter, x, introduced by Eo *et al.* [29]. The value of x for our samples is on the order of 10^{-4} around 4 K for the [110] surface sample and shrinks exponentially with cooling. This indicates that the surface channel is at least 10^4 times more conductive than the bulk, therefore we can conclude that the bulk channel does not contribute to our low-temperature magnetotransport studies.

Magnetoresistance—$\mathrm{MR} \equiv 100\% \times [R(B) - R(0)]/R(0)$ for resistance R at magnetic field B—was measured using Quantum Design Dynacool with a built-in resistance bridge using 1-μA excitation. The direction of the field was controlled using a horizontal (single axis) rotator insert with in-plane and out-of-plane rotator pucks. Resistance data below 1.8 K were measured in a Quantum Design physical property measurement system using an adiabatic demagnetization accessory and a built-in resistance bridge using 100-nA excitation.

III. SURFACE CORBINO DISK ANGULAR MAGNETORESISTANCE

Measurements of the angle dependence of MR show three distinct regions of angular response that map well to temperature-dependent changes in the zero-field resistance, as shown in Fig. 2. The correlation between the crossover in the angle dependence in MR and the plateau in low-temperature electrical resistance associated with surface states confirms that these regions are given by a low-temperature surface MR ($T \leqslant 4$ K), high-temperature bulk MR ($T \geqslant 10$ K), and intermediate mixed behavior, as described by our previous results which separate the bulk and surface transport contributions using the inverted resistance method [17].

To visualize the change in the angle dependence, we normalized the MR by the maximum value of $\mathrm{MR}(\theta)$ for each angle sweep at constant temperature and field. At high temperatures, above the resistance plateau, the electrical transport is predominantly through the bulk. In this regime, when magnetic field is applied in plane of the Corbino disk, the component of MR attributable to Lorentz force is at a minimum since the component of the current perpendicular to the magnetic field is at a minimum. This is reflected in Figs. 2(a) and 2(c) for temperatures above 8 K by roughly 50% reduction in MR for the field along the current direction in comparison to the field fully perpendicular to the current. At temperatures below 5 K, in contrast, results from surface angular MR reveal a strong dependence on field direction relative to the principle crystallographic axes, rather than the 2D current direction, as

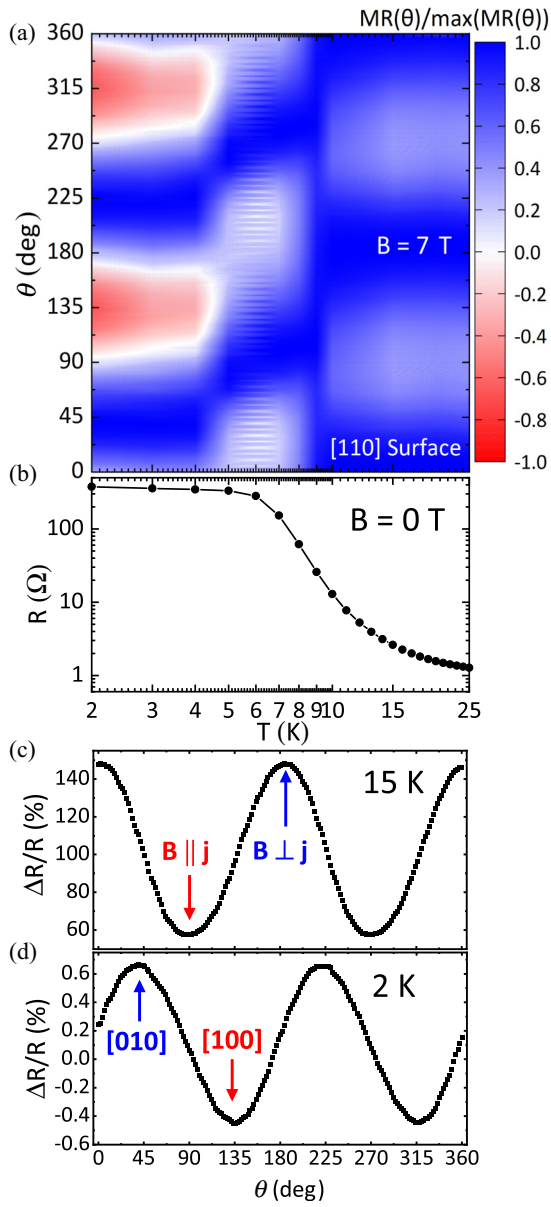

FIG. 2. Crossover in angular magnetoresistance symmetry as shown in the normalized angle dependence of MR from 25 to 2 K for current in the [110] surface with field swept in the *a*-*b* plane. (a) Angle sweep vs temperature color plot of magnetoresistance normalized to the maximum magnetoresistance for each isotherm angle sweep at 7-T magnetic field with angle sweep depicted in Fig. 1(c). (b) Zero field resistance showing the plateau on cooling coinciding with symmetry change in angular magnetoresistance and crossover from bulk to surface dominated transport regime according to inverted resistance measurements [17]. (c), (d) 7-T magnetoresistance angle sweep at 15 and 2 K corresponding to vertical line cuts of the color plot in panel (a) without normalization.

depicted in Fig. 2(d). In this temperature range, the in-plane and out-of-plane MRs are comparable and therefore inconsistent with suppression of Lorentz force on charge carriers. This result seems to rule out the Drude contribution expected from a 2DEG from playing a significant role in the surface transport properties of $FeSb_2$.

The low-temperature MR field dependence of two corbino samples with [110] and [101] surface geometries is presented in Figs. 3(a) and 3(b), respectively, for field orientations pointed along each principal crystal axis. The 2-K field response is characterized by a negative MR at low fields for all cases, most pronounced for fields along [100], and a positive MR for larger fields. Near 10 T, the [101] surface sample MR enters a high-field region characterized by a growing negative MR contribution which may be the reprisal of the low-field negative MR due to the saturation of the positive MR component.

To understand the angle dependence of these samples, we compare magnetic field rotations out of the plane of the surface [Figs. 3(d) and 3(e)] and magnetic field rotations in the plane of the surface [Figs. 3(g) and 3(h)]. In order to align visually the angles for in-plane and out-of-plane angle sweeps at 180°, we define $\theta' = 90 - \theta$ and normalize to the common direction between in-plane and out-of-plane angle sweeps. For example, $R/R_{[1\bar{1}0]}(\theta = 180^\circ) = R/R_{[1\bar{1}0]}(\phi = 180^\circ) = 1$ for the [110] surface and $R/R_{[10\bar{1}]}(\theta = 180^\circ) = R/R_{[10\bar{1}]}(\phi = 180^\circ) = 1$ for the [101] surface. The [100], [010], and [001] directions are annotated on the plots for Figs. 3(d)–3(h) for clarity. For both surfaces and all field values, the amplitude of the angle dependence for field sweeps out of plane [Figs. 3(d) and 3(e)] and in plane [Figs. 3(g) and 3(h)] are comparable in magnitude with local maxima for the field along [010] and [001] field directions. This further highlights the lack of dependence of the MR on current direction and rather that there is no shift in symmetry away from the crystalline anisotropy spanning from low fields (where the negative MR component is most prominent) to high fields (where the positive MR component is most prominent). For example, for a 2D system in which there is a negative MR contribution due to spin-orbit coupled magnetic fluctuations and as positive MR contribution due to Lorentz force on free carriers, we would expect that the MR anisotropy would shift from crystalline anisotropy at low fields to a high-field dependence on the field relative to current direction. Such a scenario is not consistent with our observations.

We can also consider the potential extrinsic effects from Sb inclusions where, as pointed out by Tang *et al.* [31], Sb may crystallize with a preferred orientation relative to the $FeSb_2$ structure and may give rise to extrinsic angular dependent physical properties that appear to be intrinsic to $FeSb_2$. We can rule this contribution out since, as discussed in Sec. II, we took care to avoid antimony inclusions in our samples. We also compared our results to angular magnetoresistance measurements on uniaxial transport geometries for small samples of $FeSb_2$ prepared by chemical vapor transport, a method which avoids Sb inclusions although it has not yet provided samples large enough for fabricating Corbino disk transport samples, and find good agreement with samples we have measured as well as in chemical vapor transport sample transport studies reported by Eaton *et al.* [22].

IV. COMPARISON OF THE [010] VS [001] SURFACE WITH UNIAXIAL TRANSPORT

Due to the size and shape restrictions of our samples, only the [101] and [110] surfaces have provided enough space for

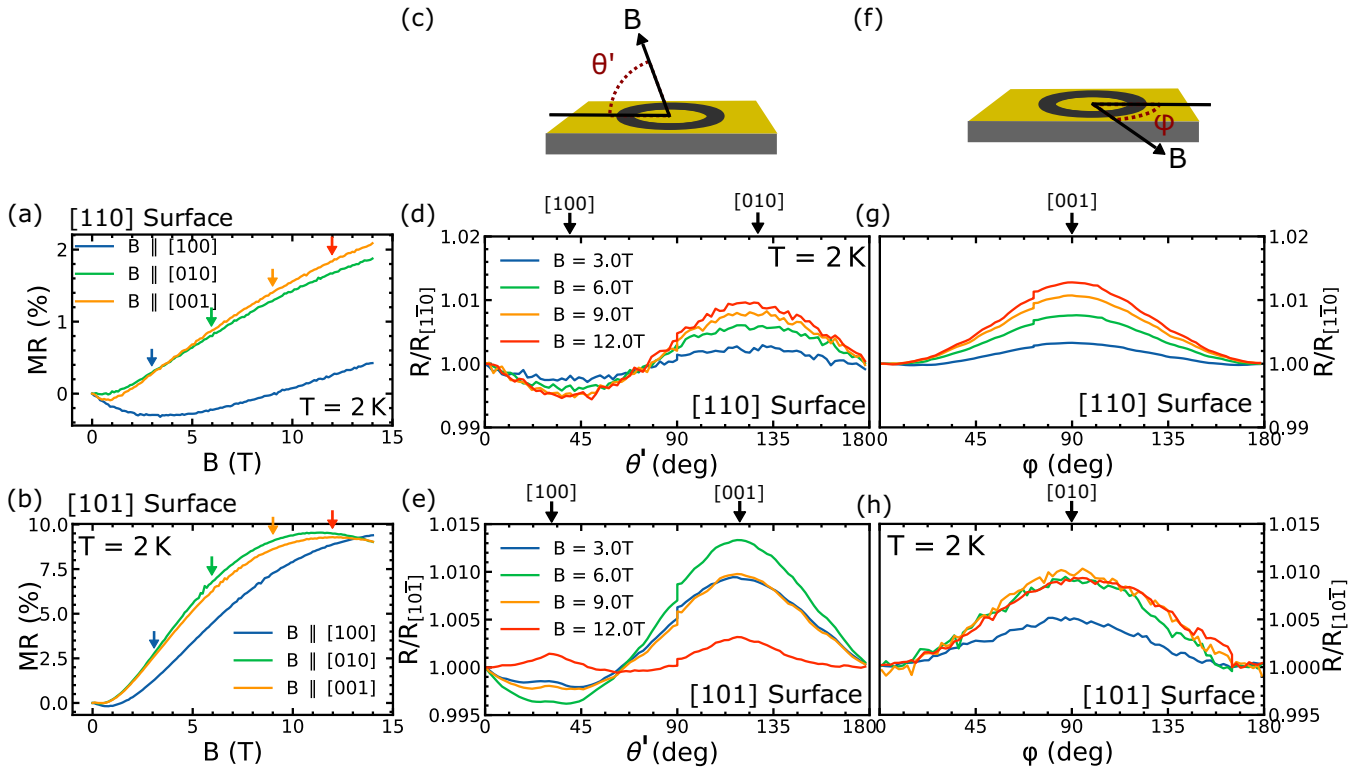

FIG. 3. (a), (b) Magnetic field dependence for the field applied along the principle crystal axes at 2 K for both current directions, [110] and [101], with arrows corresponding to fields at which angle sweeps were measured for fixed magnetic field. (c)–(e) Fixed field angle sweeps out of plane of the surface with resistance normalized to the resistance for the field applied along the corresponding in-plane magnetic field direction and angle shifted by 90° such that $\theta = 180°$ and $\phi = 0°$ correspond to the same direction and normalized value of unity. (f)–(h) Fixed field angle sweeps in plane of the surface.

patterning a Corbino disk transport geometry. Therefore, for comparison with recent ARPES results, which show surface states on the [010] surface and absence of surface states on the [001] surface [25], we examine the magnetotransport properties of these surfaces with the uniaxial current direction along the [100] direction. Although contributions from both surfaces cannot be fully isolated in this transport geometry, a combined effort of preparing a very thin and smooth surface with fine polishing was made in order to best compare the transport contributions from these surfaces for the same current and field directions. The [010] surface sample is 200 μm wide by 35 μm thin and the [001] surface sample is 400 μm wide by 20 μm thin. As shown in Fig. 4(a), the bulk-dominated transports (i.e., between 20 and 300 K) of these samples are nearly identical, confirming that the current direction is well aligned along the same direction for these two samples, since the bulk transport is well known to be anisotropic [12].

However, as shown in the inset of Fig. 4(a), the low-temperature surface-dominated transport (below 5 K, based on the plateau similar to Ref. [17]) for the [001] surface sample appears to be more insulating than that of the [010] surface sample, based on the rate of change in resistance with temperature indicating a steeper thermal activation of the low-temperature transport for the [001] surface sample. We characterize the MR response of these surfaces by again applying field along each crystallographic axis and measuring the field response. The measured anisotropy is qualitatively consistent with the Corbino disk geometry samples, as shown in Figs. 4(b) and 4(c) (i.e., the largest negative MR component is observed for the *a*-axis field, while it is minimal or negligible for the field along the *b* axis). Previous studies suggested that the observed low-field negative MR is a consequence of interference effects such as weak localization [32]. In this scenario, magnetic flux through self-intersecting loops in coherent scattering paths gives rise to interference that makes it more likely for electrons to travel in circularly localized paths [33]. This effect, however, should strongly depend on the angle between the magnetic field and the motion of charge carriers. It is also far more prevalent in 2D systems due to the lower probability of self-intersecting loops in three dimensions. The results of Figs. 4(b) and 4(c) are thus inconsistent with 2D weak localization, since self-intersecting loops perpendicular to the field along the current direction are forbidden in this transport geometry. As for three-dimensional (3D) weak localization, our results would imply an unlikely scenario in which interference effects are absent for scattering in the [010] plane but play a significant role for scattering in all other planes.

V. LOW-TEMPERATURE HOPPING CONDUCTION

The crossover from bulk to surface-dominated transport occurs around 10 K in FeSi and 5 K in $FeSb_2$, as shown by the plateau in $R(T)$ in Fig. 5(a) (a feature consistent with the bulk-to-surface crossover as established in Ref. [17]). On cooling

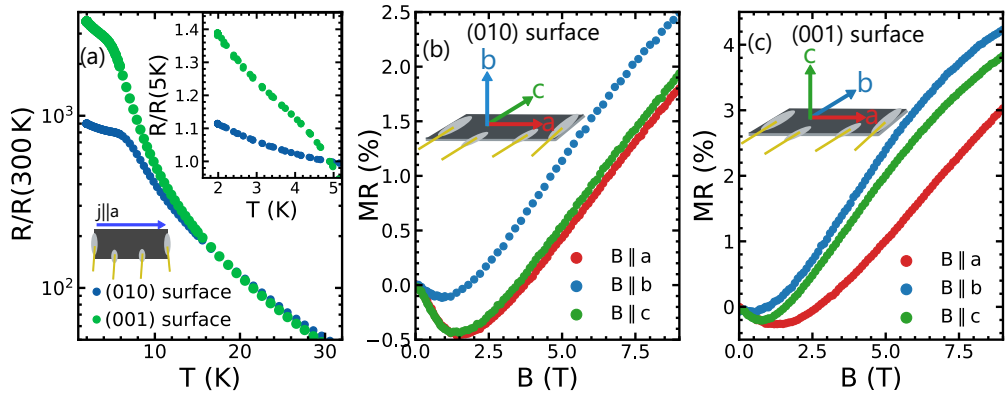

FIG. 4. Comparison of the surface MR of uniaxial c-axis current geometry for transport primarily on [010] and [001] surfaces. (a) Temperature dependence of the 300-K resistance ratio shows similar bulk transport character between the two samples with divergence below 10 K with the transition to surface dominated transport. (b), (c) Magnetic field dependence for the field along a, b, and c axes (or [100], [010], and [001], respectively) for current primarily on the (b) (010) surface and (c) (001) surface.

through the surface-dominated regime, the resistances of both [110] and [101] surfaces, as well as for [111] FeSi, continue to increase. This is atypical of the expected behavior of metallic conduction. However, the increase is also inconsistent with simple thermal activation across a charge gap, as indicated by a sublinear (rather than linear) dependence of $\ln(R)$ vs $1/T$ as shown in Fig. 5(b). Instead, the logarithmic resistance is a power law of temperature, consistent with variable-range-hopping (VRH) conduction as shown in Fig. 5(c) [although this power law in the FeSi sample deviates at lowest temperatures shown in the inset of Fig. 5(c)].

Mott VRH typically describes transport in a heavily doped or amorphous semiconductor at low temperatures, where conduction is dominated by hopping between sites with a temperature-dependent length scale. In this regime, charge carriers are localized and do not form extended states in the material (i.e., beyond the limit $k_F l > 1$). However, the inset of Fig. 5(a) shows that the sheet resistance from a geometric factor for a 2D surface Corbino disk [using dimensions in Figs. 1(a) and 1(b)]; $R_\square = 2\pi R/\ln(r_{\rm out}/r_{\rm in})$, for outer and inner radii, $r_{\rm out} = 270$ μm and $r_{\rm in} = 175$ μm] does not exceed h/e^2, the expected value for a 2D metal-to-insulator transition according to the Mott-Ioffe-Regal limit [34]. A possible explanation for this is that the assumption of a strictly 2D surface state, which was used to calculate the sheet resistance, is not valid and would therefore give a smaller effective sheet resistance due to the finite thickness of a 3D conduction channel.

The temperature dependence for VRH conduction is dimensionally dependent and takes on the form

$$\rho(T) = \rho_0 \exp\left[\left(\frac{T_{\rm VRH}}{T}\right)^p\right], \tag{1}$$

where $p = 1/(d+1)$ for a d-dimensional system (except $p = 1/2$ for Coulomb-gapped systems) and $k_B T_{\rm VRH} = \beta/[g(\mu)a^d]$ is the energy scale of the hopping channel with $g(\mu)$ the density of states, hopping length scale α, and numerical co-

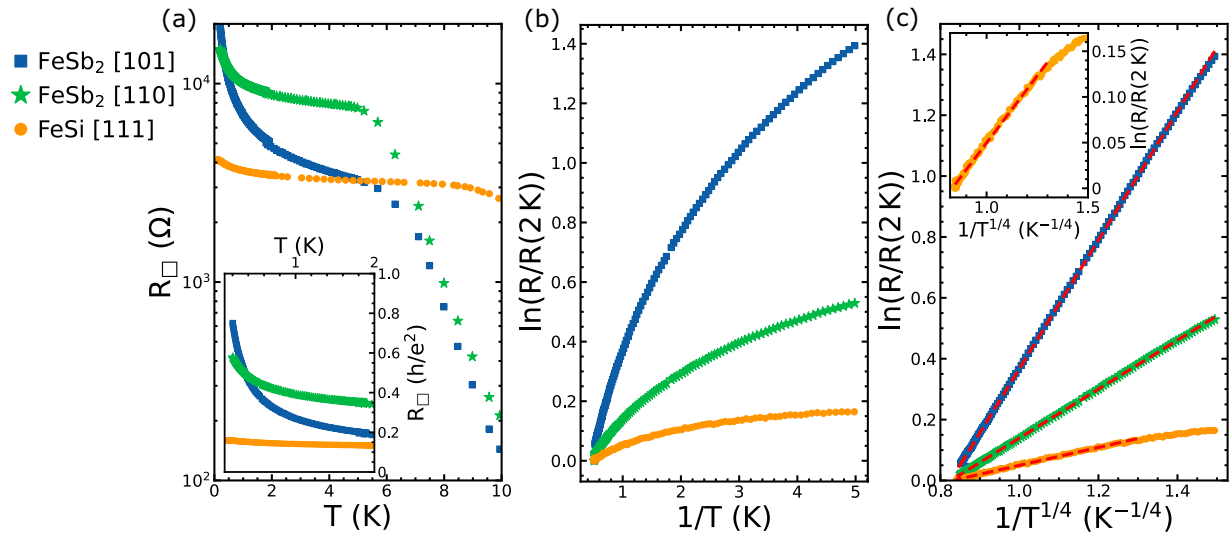

FIG. 5. (a) Extended sheet resistance measurement to low temperature on semilog scale with inset linear scale in units of h/e^2 for $FeSb_2$ [101] (blue squares), $FeSb_2$ [110] (green stars), and FeSi [111] (orange circles). (b) Sublinear dependence of logarithmic resistance on inverse temperature. (c) Power dependence of logarithmic resistance on inverse temperature with exponent of 1/4 fit (red dashed lines) to extract $T_{\rm VRH}$ for each surface.

TABLE I. Summary of low-temperature hopping transport in FeSi and $FeSb_2$.

Sample	T_{VRH} (K)	$R_\square$ (h/e^2) $T = 2$ K	$R_\square$ (h/e^2) $T = 0.2$ K
$FeSb_2$ [101]	19.8	0.348	0.751
$FeSb_2$ [110]	0.416	0.197	0.578
FeSi [111]	0.0075	0.135	0.158

efficient β [35]. This exponential power law readily describes well-known systems, such as the cases of $p = 1/4$ scaling of 3D VRH in p-type Si [36], $p = 1/3$ scaling of 2D VRH in $GaAs/Al_xGa_{1-x}As$ quantum wells [37,38], and the crossover from $p = 1/d + 1$ to $1/2$ in oxides with strong Coulomb interactions [39] and heavily irradiated graphene [40].

A $p = 1/4$ power law describes the logarithmic resistance well for the full temperature range below the crossover to the surface dominated regime, as shown in Fig. 5(c), although the FeSi sample deviates towards more conducting behavior at lowest temperatures (for more details in finding the appropriate power law, see Supplemental Material [28] and Ref. [41]). The deviation of the FeSi surface resistance from the $p = 1/4$ law at the lowest temperatures may indicate the onset of an additional conduction channel or a crossover between hopping regimes. Previous studies have shown that FeSi surfaces grown under different conditions can exhibit metallic conduction [14], suggesting that a parallel extended channel may persist in some samples. Alternatively, the deviation could reflect the emergence of the Efros-Shklovskii hopping regime ($p = 1/2$) expected when Coulomb interactions open a soft gap at the Fermi level [41]. Either scenario is consistent with a progressive delocalization of the surface states relative to the more strongly localized $FeSb_2$ surfaces. The temperature scale T_{VRH} for hopping conduction in these three samples varies dramatically as shown in Table I, with T_{VRH} for FeSi being over 2000 times smaller than that of the $FeSb_2$ [101] surface, despite having a conductivity of the same order of magnitude. For reference, while the sheet resistance of $FeSb_2$ and FeSi surfaces showing VRH conduction in this study is in the range of 0.158 to 0.751 h/e^2, SmB_6 surfaces showing metallic conduction have significantly smaller sheet resistance values of 0.0003 to 0.085 h/e^2 [30].

While it is surprising for an expectedly 2D surface state to exhibit 3D hopping character, the apparent contradiction is not unique. For example, Septianto *et al.* [42] reported a $p = 1/4$ power law for VRH in a 2D superlattice of PbS quantum dots, a 2D nanoscale network exhibiting 3D-like conduction. Other apparent violations of the $p = 1/3$ power law scaling in 2D systems have been described using an assumed temperature dependence of the resistance prefactor, ρ_0 [43,44]. In the case of the disordered surface states of the topological Kondo insulator candidate, SmB_6, reported by Batkova *et al.* [45], a temperature-independent parallel resistance channel was introduced to fit the data to a $p = 1/3$ power law. As another example of a disordered surface state on a bulk 3D insulator, such results are important for understanding our current work. Therefore, we examine the data separately (see Supplemental Material [28] Fig. S5), finding a similar $p = 1/4$ power law when assuming no parallel conduction channels are present. These deviations from $p = 1/3$ scaling in 2D (or quasi-2D) systems are important for understanding the limits of the standard analysis for hopping conduction as well as how the effective transport length scales compare with the physical dimensions (e.g., effective thickness) of these samples.

VI. FITTING MR TO HOPPING AND LOCAL MOMENT SCATTERING MODELS

The low-temperature MR is inconsistent with conventional orbital (Lorentz force driven) MR as established by the angle dependence and negative MR at low fields. Similarly, the low-temperature resistance is consistent with hopping conduction rather than metallic transport. To reconcile these observations, we first considered the effect of magnetic field on hopping conduction. In semiconductors doped towards their insulator-to-metal transitions like n-Ge and various III-V systems, a large, exponential dependence of resistance on magnetic field has been shown [46–49]. This effect is attributed to the shrinking of the spatial extent of localized states such that the overlap between neighboring impurity sites is reduced and therefore hopping conduction is suppressed [35]. This effect is largest for lightly doped semiconductors in which overlap at zero field is already small, so it is well understood to scale with the effective impurity radius and density of states at the Fermi level and takes the form

$$\left(\frac{\rho(H)}{\rho(0)}\right)_{VRH} = \exp\left[\frac{tae^2}{Nc^2\hbar^2}\left(\frac{T_{VRH}}{T}\right)^{3/4}H^2\right] \qquad (2)$$

where a is the impurity site radius, N is the impurity concentration, and $t = 5/2016$ is a numerical coefficient [35]. This field dependence only accounts for the increase in resistance, while in some hopping conduction systems (and in the data we present), a decrease in resistance at low fields is observed. In some heavily doped semiconductors, negative MR has been attributed to the Zeeman effect in which carriers in the upper Zeeman state have an increased wave-function overlap with neighboring states. This effect was proposed by Fukuyama and Yosida [50] and used to describe the low-field MR of n-type GaAs [51]. However, this effect should scale with temperature proportional to $T^{1/4}$ (i.e., decreasing with cooling) in contradiction with $FeSb_2$ results showing a negative MR component increasing with cooling as shown in Fig. 6. Negative MR in variable-range-hopping systems is typically attributed to quantum interference from self-intersecting loops within paths connecting hopping sites [35,52]. This interference, as discussed in a previous section, should depend on field direction relative to current, which is absent in the MR of $FeSb_2$.

A possible explanation for the anisotropic negative MR observed in $FeSb_2$ is the effect of local moment scattering, which could be anisotropic with respect to the crystal field. The usual s-d scattering picture of conduction electrons coupling to local moments works well for understanding the origin of negative MR in metals with magnetic impurities. Although the validity of applying s-d scattering models to VRH systems is not straightforward, experimental evidence of the coupling of transport to local magnetic moments in VRH systems is clearly observed for dilute magnetic semiconductors, and even

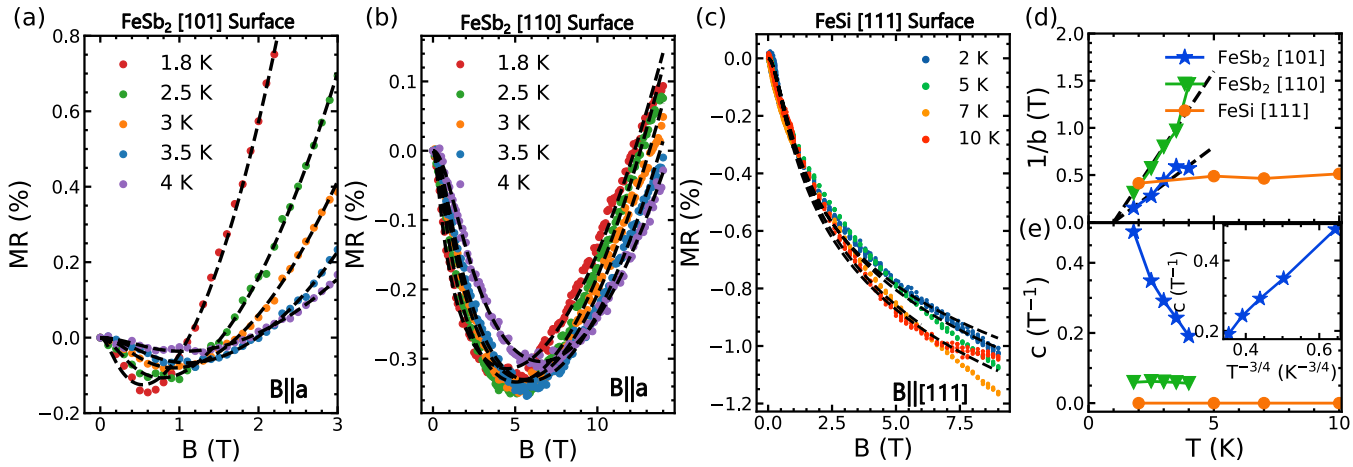

FIG. 6. Results from fitting the MR of (a) $FeSb_2$ [101] surface MR with the field along the a axis, (b) $FeSb_2$ [110] surface MR with the field along the a axis, and (c) FeSi [111] surface MR with the field along the [111] direction to Eq. (4) with black dashed lines representing lines of best fit. (d), (e) Extracted values of the magnetic field scale of (d) local moment scattering and (e) suppression of hopping conduction. The inset of panel (e) shows that $FeSb_2$ [101] fit results most closely resemble the expected temperature scaling for the field scale of hopping conduction suppression.

at the surface of FeSi [21,53,54]. Therefore, we consider the contribution of magnetic impurities to the negative MR of our samples at low temperatures.

Bulk $FeSb_2$ does not exhibit large magnetocrystalline anisotropy, as its ground state is singlet [12,25]. However, when electron doped by Te substitution into a bulk metal, for example, the magnetic properties become extremely anisotropic with the [100] magnetic easy axis [55]. Local moment scattering in metals, from second order perturbation theory, should give a $-M^2$ (for M magnetization of local moment) contribution to MR at small magnetic fields and thus follow a Curie-Weiss scaling with temperature for negative quadratic MR. Although this scaling has been shown to work well to describe Cu-Mn alloys [56,57], it is limited and incomplete in describing local moment scattering for some systems in which impurity scattering from local moments plays a role. A calculation based on the third-order expansion of the s-d exchange interaction is used here, adapted by Khosla and Fischer [58] from early theory work on tunnel junctions with transition metal impurities [59]:

$$\left(\frac{\Delta\rho(H)}{\rho(0)}\right)_{KF} = -A_1 J \rho_F \ln\left[1+\left(\frac{g_0\mu}{\alpha k_B T}\right)^2 B^2\right]. \quad (3)$$

The original Khosla and Fischer paper [58] also gives a quadratic positive MR contribution in addition to this negative component from local moment scattering. The authors make it clear that a Lorentz force contribution is not responsible for the observed positive MR as they observe positive longitudinal MR of the same order as transverse, similar to the data we present in this paper. They suggest a possible two-band scenario in which the relative band populations, and therefore the effective resistance, change with field to give an overall positive quadratic component. However, in the heavily doped regime (in which N/a is large) or at small fields, Eq. (2) can be expanded to first order in small argument to give a quadratic MR which is consistent with the observed MR of Khosla and Fischer. Giving a complete expression for carriers hopping in a doped semiconductor, in which local moments play a leading role in the scattering of charge carriers, we have

$$\frac{\rho(H)}{\rho(0)} = -a\ln(1+b^2B^2) + \exp(c^2B^2), \quad (4)$$

where the field scales of local moment scattering, i.e., b from Eq. (3), should scale with T^{-1}, and field scales of local wavefunction shrinkage, i.e., c from Eq. (2), should scale with $T^{-3/4}$.

The temperature dependence of MR in the surface transport regime agrees well with the expected behavior from Eq. (4) for the [101] surface of $FeSb_2$ as shown in Fig. 6. The field scale of the negative MR component evolves linearly with temperature while the field dependence of the hopping contribution (positive MR component) scales as $T^{3/4}$. The temperature evolution of the hopping field scale, c, for the $FeSb_2$ [110] and FeSi [111] surfaces appears to be inconsistent with the expected scaling in this temperature range ($T \geqslant 2$ K). This can be attributed to the small hopping temperature relative to the temperature range being measured in Fig. 6, such that the surface carriers are too delocalized to be sensitive to the small changes in localized state wave functions with applied field. For both $FeSb_2$ samples, we find good agreement with the model from Khosla and Fischer [58], which does not have explicit dependence on the nature of conduction. The FeSi sample, however, shows no agreement with the temperature dependence expected from the Kholsla and Fischer model. This is not surprising since there is a built-in assumption of noninteracting local moments in the model, which contrasts with the reported magnetic order at the surface of FeSi that plays a significant role in the observed negative MR [18,20,21].

While the identification of local moment scattering as the origin of the negative MR is based primarily on transport signatures, magnetization measurements on FeSi and $FeSb_2$ crystals from the same growth batch reveal a low-temperature magnetic response that scales with surface area, directly im-

plicating localized surface moments. A detailed account of these magnetic measurements is reported for FeSi (see, e.g., Ref. [21]), the subject of an ongoing investigation in $FeSb_2$.

VII. DISCUSSION

The transport character of our $FeSb_2$ and FeSi samples is consistent with a disordered surface conduction layer with an effective thickness larger than the characteristic length scale of the hopping channel. This result provides good evidence that $FeSb_2$ and FeSi are not strong topological insulators, since our transport results show conduction by 3D localized states unlike the 2D metallic (extended) states expected at the surface of a strong topological insulator. Without knowing the dielectric properties of $FeSb_2$, it is difficult to estimate the length scale of the hopping channel, l_{hop}, but it may be as small as a few or tens of nanometers and decreases with temperature as $l_{\mathrm{hop}} \propto a_{\mathrm{eff}}(\frac{T}{T_{\mathrm{VRH}}})^{1/4}$ for some effective Bohr radius, a_{eff} [35]. While the value of T_{VRH} varies by orders of magnitude among these samples, it should be noted that l_{hop} may only vary by a factor of 2.6 in between the [110] and [101] surfaces of $FeSb_2$ and a factor of 7.2 between $FeSb_2$ and FeSi, assuming the same value of a_{eff} (the value of which depends on band structure and, in mixed-valence insulators, can be orders of magnitude smaller than expected based on effective mass alone [60]).

The origin of this surface transport channel is not fully understood. Based on the crystalline anisotropy found in the surface MR, and the fact that spectroscopic observations of surface states were measured on surfaces cleaved in vacuum, a disordered conducting oxide layer can be ruled out. A recent ARPES and *ab initio* combined study by Chikina *et al.* concluded that small structural distortions of a few percent of the bulk lattice parameters is enough to shift a bulk band near the Fermi level to match observed surface state dispersion results [24]. These results would suggest that these surface states appear due to some weak structural distortion that is not present in the bulk. It is important to note that while ARPES transport studies have demonstrated coherent surface states on certain clean facets [15,24,25], such states are not necessarily expected to give rise to macroscopic metallic transport if such states are not topologically protected. The finite thickness and disordered character of the conducting surface layer inferred from 3D hopping conduction imply that any nontopological surface bands are localized by surface disorder. This scenario is consistent with Anderson localization of trivial surface states once the mean free path is reduced below the localization length. Furthermore, we emphasize that the conclusion that $FeSb_2$ is not a strong topological insulator is based on the behavior of as-grown surfaces studied here and on transport signatures of localized, three-dimensional conduction. While transport alone cannot directly establish the topological classification, the absence of a two-dimensional metallic surface channel, together with the facet-dependent and nontopological surface states observed in ARPES and *ab initio* calculations [24,25], supports our interpretation that the conducting layer is a disordered, trivial surface state rather than a protected topological one.

While our measurements do not directly image surface disorder, the emergence of variable-range-hopping conduction is consistent with carrier localization in a disordered potential. The strong crystalline anisotropy of the surface magnetoresistance further excludes an amorphous oxide layer and points instead to a structurally distorted crystalline surface. Together with the vacancy disorder and symmetry reduction reported by Du *et al.* [61], these results indicate that the surface conduction channel arises from a disordered but crystalline layer of finite thickness rather than from an ideal, stoichiometric termination. In this series of experiments investigating structural defects via scanning transmission electron microscopy and neutron scattering measurements, Du *et al.* reported structural distortions due to both Fe and Sb vacancies in all measured samples of $FeSb_2$ with various growth conditions. These vacancies are frequent enough to show site occupations as small as 82% in some Sb sites and 94% in some Fe sites. It was reported that samples with these levels of vacancies also show a monoclinic distortion that is evidenced by forbidden reflections in neutron scattering, indicating some reduced symmetry. It is worth noting that, while Du *et al.* suggest these defects contribute in-gap impurity states that modify bulk physical property measurements, recent measurements of the bulk resistivity using the inverted resistance method show no sign of bulk impurity conduction [17]. This implies that defects present in the bulk may contribute to scattering processes but do not form an impurity band, and that somehow the bulk electronic gap is incredibly robust to these defects. Therefore, the presence of trivial surface states seems to suggest that either the robustness of the bulk breaks down or the structural distortion due to vacancies is stronger near the surface. Future work to directly probe structural disorder or reconstruction of the surface is needed to further understand the correlation between the surface transport properties and disorder in these samples.

VIII. CONCLUSION

Magnetotransport measurements of two isolated surfaces of the candidate *d*-electron topological Kondo insulator $FeSb_2$ were measured using both Corbino and oriented four-wire geometries. Our measurements of field-angle-dependent low-temperature electrical transport properties point to the following conclusions.

(1) There is a crossover from orbital-dominated bulk MR at high temperatures, to a surface state angular response dominated by crystalline anisotropy at low temperatures.

(2) There is a low-temperature negative MR that is inconsistent with weak localization.

(3) Electrical transport properties are sensitive to the conducting surface, with (010) and (001) comparisons consistent with ARPES results [25].

(4) A surface hopping transport behavior is best described by power laws consistent with 3D conduction.

(5) A combined hopping and local moment scattering model best describes the temperature and magnetic field dependence of the surface MR.

We show that these results are qualitatively similar to the surface transport properties measured on the [111] surface of

FeSi, which also exhibits low-temperature three-dimensional variable-range-hopping conduction and magnetic scattering. This suggests that the surface states of $FeSb_2$ are best described as a disordered semiconducting layer of finite thickness, instead of a two-dimensional electron gas as expected for the surface states of a strong topological insulator.

ACKNOWLEDGMENTS

Research at the University of Maryland was supported by AFOSR Grant No. FA9950-22-1-0023, NSF Grant No. DMR2303090, the Gordon and Betty Moore Foundation's EPiQS Initiative Grant No. GBMF9071, the NIST Center for Neutron Research, and the Maryland Quantum Materials Center.

DATA AVAILABILITY

The data that support the findings of this article are not publicly available upon publication because it is not technically feasible and/or the cost of preparing, depositing, and hosting the data would be prohibitive within the terms of this research project. The data are available from the authors upon reasonable request.

[1] M. Dzero, J. Xia, V. Galitski, and P. Coleman, Topological Kondo insulators, Annu. Rev. Condens. Matter Phys. **7**, 249 (2016).

[2] A. Menth, E. Buehler, and T. H. Geballe, Magnetic and semiconducting properties of SmB_6, Phys. Rev. Lett. **22**, 295 (1969).

[3] R. M. Martin and J. W. Allen, Theory of mixed valence: Metals or small gap insulators (invited), J. Appl. Phys. **50**, 7561 (1979).

[4] S. Rößler, T.-H. Jang, D.-J. Kim, L. H. Tjeng, Z. Fisk, F. Steglich, and S. Wirth, Hybridization gap and Fano resonance in SmB_6, Proc. Natl. Acad. Sci. USA **111**, 4798 (2014).

[5] T. Takabatake, F. Iga, T. Yoshino, Y. Echizen, K. Katoh, K. Kobayashi, M. Higa, N. Shimizu, Y. Bando, G. Nakamoto, H. Fujii, K. Izawa, T. Suzuki, T. Fujita, M. Sera, M. Hiroi, K. Maezawa, S. Mock, H. Löhneysen, A. Brückl, *et al.*, Ce- and Yb-based Kondo semiconductors, J. Magn. Magn. Mater. **177-181**, 277 (1998).

[6] H. Weng, J. Zhao, Z. Wang, Z. Fang, and X. Dai, Topological crystalline Kondo insulator in mixed valence ytterbium borides, Phys. Rev. Lett. **112**, 016403 (2014).

[7] C.-J. Kang, J. D. Denlinger, J. W. Allen, C.-H. Min, F. Reinert, B. Y. Kang, B. K. Cho, J.-S. Kang, J. H. Shim, and B. I. Min, Electronic structure of YbB_6: Is it a topological insulator or not? Phys. Rev. Lett. **116**, 116401 (2016).

[8] C. Broyles, X. Wan, W. Cheng, D. Wu, H. Tan, Q. Xu, S. L. Gould, H. Siddiquee, L. Xiao, R. Chen, W. Lin, Y. Wu, P. Regmi, Y. S. Eo, J. Liu, Y. Chen, B. Yan, K. Sun, and S. Ran, High temperature surface state in Kondo insulator $U_3Bi_4Ni_3$ Sci. Adv. **11**, eadq9952 (2025).

[9] Y. S. Eo, A. Rakoski, J. Lucien, D. Mihaliov, u. Kurdak, P. F. S. Rosa, and Z. Fisk, Transport gap in SmB_6 protected against disorder, Proc. Natl. Acad. Sci. USA **116**, 12638 (2019).

[10] C. E. Matt, H. Pirie, A. Soumyanarayanan, Y. He, M. M. Yee, P. Chen, Y. Liu, D. T. Larson, W. S. Paz, J. J. Palacios, M. H. Hamidian, and J. E. Hoffman, Consistency between ARPES and STM measurements on SmB_6, Phys. Rev. B **101**, 085142 (2020).

[11] P. Hlawenka, K. Siemensmeyer, E. Weschke, A. Varykhalov, J. Sánchez-Barriga, N. Y. Shitsevalova, A. V. Dukhnenko, V. B. Filipov, S. Gabáni, K. Flachbart, O. Rader, and E. D. L. Rienks, Samarium hexaboride is a trivial surface conductor, Nat. Commun. **9**, 517 (2018).

[12] C. Petrovic, Y. Lee, T. Vogt, N. D. Lazarov, S. L. Bud'ko, and P. C. Canfield, Kondo insulator description of spin state transition in $FeSb_2$, Phys. Rev. B **72**, 045103 (2005).

[13] Z. Schlesinger, Z. Fisk, H.-T. Zhang, and M. Maple, Is FeSi a Kondo insulator? Physica B **237-238**, 460 (1997).

[14] Y. Fang, S. Ran, W. Xie, S. Wang, Y. S. Meng, and M. B. Maple, Evidence for a conducting surface ground state in high-quality single crystalline FeSi, Proc. Natl. Acad. Sci. USA **115**, 8558 (2018).

[15] K.-J. Xu, S.-D. Chen, Y. He, J. He, S. Tang, C. Jia, E. Yue Ma, S.-K. Mo, D. Lu, M. Hashimoto, T. P. Devereaux, and Z.-X. Shen, Metallic surface states in a correlated d-electron topological Kondo insulator candidate $FeSb_2$, Proc. Natl. Acad. Sci. USA **117**, 15409 (2020).

[16] S. Changdar, S. Aswartham, A. Bose, Y. Kushnirenko, G. Shipunov, N. C. Plumb, M. Shi, A. Narayan, B. Büchner, and S. Thirupathaiah, Electronic structure studies of FeSi: A chiral topological system, Phys. Rev. B **101**, 235105 (2020).

[17] Y. S. Eo, K. Avers, J. A. Horn, H. Yoon, S. R. Saha, A. Suarez, M. S. Fuhrer, and J. Paglione, Extraordinary bulk-insulating behavior in the strongly correlated materials FeSi and $FeSb_2$, Appl. Phys. Lett. **122**, 233102 (2023).

[18] Y. Ohtsuka, N. Kanazawa, M. Hirayama, A. Matsui, T. Nomoto, R. Arita, T. Nakajima, T. Hanashima, V. Ukleev, H. Aoki, M. Mogi, K. Fujiwara, A. Tsukazaki, M. Ichikawa, M. Kawasaki, and Y. Tokura, Emergence of spin-orbit coupled ferromagnetic surface state derived from Zak phase in a nonmagnetic insulator FeSi, Sci. Adv. **7**, eabj0498 (2021).

[19] A. J. Breindel, Y. Deng, C. M. Moir, Y. Fang, S. Ran, H. Lou, S. Li, Q. Zeng, L. Shu, C. T. Wolowiec, I. K. Schuller, P. F. S. Rosa, Z. Fisk, J. Singleton, and M. B. Maple, Probing FeSi, a d-electron topological Kondo insulator candidate, with magnetic field, pressure, and microwaves, Proc. Natl. Acad. Sci. USA **120**, e2216367120 (2023).

[20] Y. Deng, Y. Yan, H. Wang, E. Lee-Wong, C. M. Moir, Y. Fang, W. Xie, and M. B. Maple, Possible surface magnetism in the topological Kondo insulator candidate FeSi, Phys. Rev. B **108**, 115158 (2023).

[21] K. E. Avers, Y. S. Eo, H. Yoon, J. A. Horn, S. R. Saha, A. Suarez, P. Zavalij, and J. Paglione, Disordered two-dimensional ferromagnetism at the surface of FeSi, Phys. Rev. B **110**, 134416 (2024).

[22] A. G. Eaton, N. J. M. Popiel, K.-J. Xu, A. J. Hickey, H. Liu, M. C. Hatnean, G. Balakrishnan, G. F. Lange, R.-J. Slager, Z.-X. Shen, and S. E. Sebastian, Electrical transport signatures of metallic surface state formation in the strongly-correlated insulator $FeSb_2$, arXiv:2403.04550.

[23] I. I. Mazin, K. Koepernik, M. D. Johannes, R. González-Hernández, and L. Šmejkal, Prediction of unconventional magnetism in doped $FeSb_2$, Proc. Natl. Acad. Sci. USA **118**, e2108924118 (2021).

[24] A. Chikina, J.-Z. Ma, W. H. Brito, S. Choi, P. Sémon, A. Kutepov, Q. Du, J. Jandke, H. Liu, N. C. Plumb, M. Shi, C. Petrovic, M. Radovic, and G. Kotliar, Correlated electronic structure of colossal thermopower $FeSb_2$: An ARPES and *ab initio* study, Phys. Rev. Res. **2**, 023190 (2020).

[25] H. Li, G. Wang, N. Ding, Q. Ren, G. Zhao, W. Lin, J. Yang, W. Yan, Q. Li, R. Yang, S. Yuan, J. D. Denlinger, Z. Wang, X. Zhang, L. A. Wray, S. Dong, D. Qian, and L. Miao, Spectroscopic evidence of spin-state excitation in d-electron correlated semiconductor $FeSb_2$, Proc. Natl. Acad. Sci. USA **121**, e2321193121 (2024).

[26] $FeSb_2$ crystal structure, Springer Materials (2023), https://materials.springer.com/isp/crystallographic/docs/sd_1008518.

[27] C. Petrovic, J. W. Kim, S. L. Bud'ko, A. I. Goldman, P. C. Canfield, W. Choe, and G. J. Miller, Anisotropy and large magnetoresistance in the narrow-gap semiconductor $FeSb_2$, Phys. Rev. B **67**, 155205 (2003).

[28] See Supplemental Material at http://link.aps.org/supplemental/10.1103/5jfb-8p78 for further details about sample orientation and preparation, transport analysis, and comments.

[29] Y. S. Eo, K. Sun, Ç. Kurdak, D.-J. Kim, and Z. Fisk, Inverted resistance measurements as a method for characterizing the bulk and surface conductivities of three-dimensional topological insulators, Phys. Rev. Appl. **9**, 044006 (2018).

[30] Y. S. Eo, S. Wolgast, A. Rakoski, D. Mihaliov, B. Y. Kang, M. S. Song, B. K. Cho, M. C. Hatnean, G. Balakrishnan, Z. Fisk, S. R. Saha, X. Wang, J. Paglione, and U. Kurdak, Comprehensive surface magnetotransport study of SmB_6, Phys. Rev. B **101**, 155109 (2020).

[31] F. Tang, Q. Du, C. Petrovic, W. Zhang, M. He, and L. Zhang, Negative differential resistance and quantum oscillations in $FeSb_2$ with embedded antimony, Chin. Phys. B **28**, 037104 (2019).

[32] H. Takahashi, R. Okazaki, Y. Yasui, and I. Terasaki, Low-temperature magnetotransport of the narrow-gap semiconductor $FeSb_2$, Phys. Rev. B **84**, 205215 (2011).

[33] S. Datta, *Electronic Transport in Mesoscopic Systems* (Cambridge University Press, New York, 1995).

[34] S. Das Sarma and E. H. Hwang, Two-dimensional metal-insulator transition as a strong localization induced crossover phenomenon, Phys. Rev. B **89**, 235423 (2014).

[35] B. I. Shklovskii and A. L. Efros, *Electronic Properties of Doped Semiconductors* (Springer-Verlag, Berlin, 1984), Chap. 9, pp. 202–212.

[36] W. N. Shafarman and T. G. Castner, Critical behavior of Mott variable-range hopping in Si:As near the metal-insulator transition, Phys. Rev. B **33**, 3570 (1986).

[37] R. L. J. Qiu, X. P. A. Gao, L. N. Pfeiffer, and K. W. West, Connecting the reentrant insulating phase and the zero-field metal-insulator transition in a 2D hole system, Phys. Rev. Lett. **108**, 106404 (2012).

[38] A. Chakhmane, H. El Idrissi, A. El Kaaouachi, M. Errai, A. El Oujdi, and A. Echchelh, Variable range hopping in a dilute GaAs/AlGaAs hole system, J. Korean Phys. Soc. **75**, 389 (2019).

[39] R. Rosenbaum, Crossover from Mott to Efros-Shklovskii variable-range-hopping conductivity in In_xO_y thin films, Phys. Rev. B **44**, 3599 (1991).

[40] E. Zion, A. Haran, A. Butenko, L. Wolfson, Y. Kaganovskii, T. Havdala, A. Sharoni, D. Naveh, V. Richter, M. Kaveh, E. Kogan, and I. Shlimak, Localization of charge carriers in monolayer graphene gradually disordered by ion irradiation, Graphene **4**, 45 (2015).

[41] A. G. Zabrodskii, The Coulomb gap: The view of an experimenter, Philos. Mag. B **81**, 1131 (2001).

[42] R. D. Septianto, R. Miranti, T. Kikitsu, T. Hikima, D. Hashizume, N. Matsushita, Y. Iwasa, and S. Z. Bisri, Nat. Commun. **14**, 2670 (2023).

[43] L. Li, G.-H. Kim, K. J. Thomas, and D. A. Ritchie, Hopping conduction and magnetoresistance of a GaAs/$Al_xGa_{1-x}As$ quantum well with embedded InAs dots, Phys. Rev. B **83**, 153304 (2011).

[44] F. W. Van Keuls, X. L. Hu, H. W. Jiang, and A. J. Dahm, Screening of the Coulomb interaction in two-dimensional variable-range hopping, Phys. Rev. B **56**, 1161 (1997).

[45] M. Batkova, I. Batko, S. Gabáni, E. Gazo, E. Konovalova, and V. Filippov, Physica B: Condensed Matter **536**, 200 (2018).

[46] W. Sasaki, Negative magnetoresistance in the metallic impurity conduction of *n*-type germanium, J. Phys. Soc. Jpn. **20**, 825 (1965).

[47] B. Sernelius and K. F. Berggren, Origin of negative magnetoresistance in heavily doped *n*-type silicon and germanium, Phys. Rev. B **19**, 6390 (1979).

[48] J. Monsterleet, B. Capoen, and G. Biskupski, Negative magnetoresistance in insulating *n*-type GaAs and localized magnetic moments, Solid State Commun. **101**, 525 (1997).

[49] A. Oiwa, S. Katsumoto, A. Endo, M. Hirasawa, Y. Iye, F. Matsukura, A. Shen, Y. Sugawara, and H. Ohno, Low-temperature conduction and giant negative magnetoresistance in III–V-based diluted magnetic semiconductor: (Ga, Mn)As/GaAs, Physica B **249-251**, 775 (1998).

[50] H. Fukuyama and K. Yosida, Negative magnetoresistance in the Anderson localized states. II. Effect of electron correlations, J. Phys. Soc. Jpn. **46**, 1522 (1979).

[51] M. Benzaquen, D. Walsh, and K. Mazuruk, Low-field magnetoresistance *ofn*-type GaAs in the variable-range hopping regime, Phys. Rev. B **38**, 10933 (1988).

[52] R. Abdia, A. El Kaaouachi, A. Nafidi, G. Biskupski, and J. Hemine, Variable range hopping conductivity and negative magnetoresistance in *n*-type InP semiconductor, Solid-State Electron. **53**, 469 (2009).

[53] A. Van Esch, L. Van Bockstal, J. De Boeck, G. Verbanck, A. S. van Steenbergen, P. J. Wellmann, B. Grietens, R. Bogaerts, F. Herlach, and G. Borghs, Interplay between the magnetic and transport properties in the III-V diluted magnetic semiconductor $Ga_{1-x}Mn_xAs$, Phys. Rev. B **56**, 13103 (1997).

[54] Y. D. Park, A. Wilson, A. T. Hanbicki, J. E. Mattson, T. Ambrose, G. Spanos, and B. T. Jonker, Magnetoresistance of Mn:Ge ferromagnetic nanoclusters in a diluted magnetic semiconductor matrix, Appl. Phys. Lett. **78**, 2739 (2001).

[55] R. Hu, V. F. Mitrović, and C. Petrovic, Magnetism and metal-insulator transition in $Fe(Sb_{1-x}Te_x)_2$, Phys. Rev. B **79**, 064510 (2009).

[56] K. Yosida, Anomalous electrical resistivity and magnetoresistance due to $s - d$ interaction in Cu-Mn alloys, Phys. Rev. **107**, 396 (1957).

[57] Y. Toyozawa, Theory of localized spins and negative magnetoresistance in the metallic impurity conduction, J. Phys. Soc. Jpn. **17**, 986 (1962).

[58] R. P. Khosla and J. R. Fischer, Magnetoresistance in degenerate CdS: Localized magnetic moments, Phys. Rev. B **2**, 4084 (1970).

[59] J. A. Appelbaum, Exchange model of zero-bias tunneling anomalies, Phys. Rev. **154**, 633 (1967).

[60] B. Skinner, Properties of the donor impurity band in mixed valence insulators, Phys. Rev. Mater. **3**, 104601 (2019).

[61] Q. Du, L. Wu, H. Cao, C.-J. Kang, C. Nelson, G. L. Pascut, T. Besara, T. Siegrist, K. Haule, G. Kotliar, I. Zaliznyak, Y. Zhu, and C. Petrovic, Vacancy defect control of colossal thermopower in $FeSb_2$, npj Quantum Mater. **6**, 13 (2021).

Supplemental Information: Magnetocrystalline Anisotropy and 3D Hopping Conduction at the Surface of $FeSb_2$

Jarryd A. Horn,[1] Yun Suk Eo,[1,2] Keenan Avers,[1] Hyeok Yoon,[1]
Ryan G. Dorman,[1,3] Shanta R. Saha,[1] and Johnpierre Paglione[1,4]

[1] *Maryland Quantum Materials Center and Department of Physics, University of Maryland, College Park, Maryland 20742, USA*
[2] *Texas Tech University Department of Physics, Lubbock, Texas 79409, USA*
[3] *University of Colorado Department of Physics, Boulder, Colorado 80309, USA*
[4] *Canadian Institute for Advanced Research, Toronto, Ontario M5G 1Z8, Canada*

(Dated: September 6, 2025)

Sample orientation and preparation

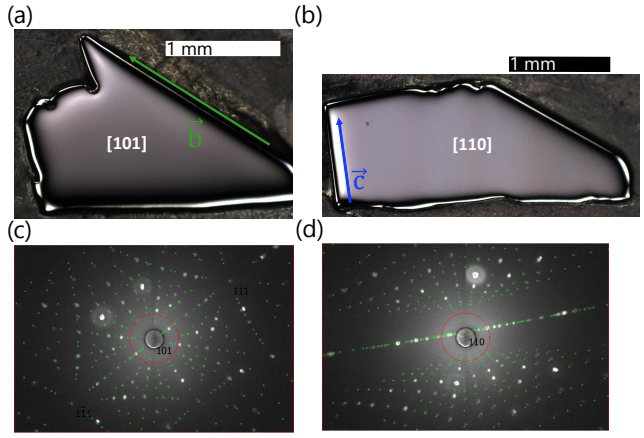

FIG. 1. Orientation of [101] and [110] surface samples from Laue diffraction. (a-b) Sample photos after polishing surface with 0.3 micron Alumina with identified edge directions aligned with crystallographic directions. (c-d) Laue diffraction images (black and white) with overlayed fit to pattern (green) to determine orientation for field rotation.

$FeSb_2$ grown by Sb flux produce large surfaces of [110] and [101] facets. Samples with these surfaces which were large enough to pattern Corbino disks were chose and these surfaces were prepared with minimally abrasive polishing to avoid producing subsurface cracks, which have been shown to contribute to surface conduction in SmB_6. To clean surfaces to be free from residual Sb flux, 0.3 micron alumina particles were used in a suspension to prepare high quality surfaces shown in figure 1a and 1b. The corresponding laue patterns in figure 1c and 1d were measured for the samples in the orientation showed in figure 1a and 1b to find the edges shown which match within 1 degree alignment the directions indicated by the arrows for precise orientation. This precision allows us to be certain that the magnetotransport symmetry is derrived from crystal symmetry with negligible shift from contributions due to the relationship between current and field which is expected in metals due to Lorentz force contribution to magnetoresistance.

Lorentz force contribution to surface and bulk

In metals, there is the expectation from Drude transport that the first order contribution to magnetotransport is the classical effect of Lorentz force on charge carriers. This is easy reconciled by suppressing magnetoresistance when the magnetic field is coincident with the current direction to give a well defined angle dependence:

$$MR = \mu^2 B^2 \sin^2(\theta) \tag{1}$$

where μ is the carrier mobility and θ is the angle between the magnetic field and current direction in a linear transport geometry. This relationship is easily derived from the classical equation of motion for a charge carrier in an electric and magnetic field. In a 2D electron gas (2DEG), this behavior is expected for θ being the angle between the magnetic field and the 2D plane (or Corbino disk in our case) in which the current is confined. This directly implies that there should be zero in-plane (positive) magnetoresistance in a 2DEG, which is inconsistant with results for all in-plane magnetoresistance field direction in the surface transport regime results shown in figure 2a and 2b.

For 3D conduction in a Corbino disk, however, the physics is the same however it can be intuitively understood that the magnetoresistance is only partially suppressed for in-plane magnetic fields, by 50% in an isotropic system. In an anisotropic 3D system, the in-plane suppression varies with direction and is determined by the relationship between the mobility components perpendicular and parallel to the magnetic field but in any case, the quadratic magnetic field dependence should always be smaller for fields in plane in comparason to the out-of-plane field dependence. This effect is observed in the high temperature magnetotransport results shown for $FeSb_2$ Corbinos in figure 2c and 2d, in which the conduction is dominated by bulk carriers. At low temperatures, however, the magnetoresistance is larger in-plane than out-of-plane for at least one direction in-plane for both samples. This directly violates the classical prediction for both 2D and 3D Drude behavior.

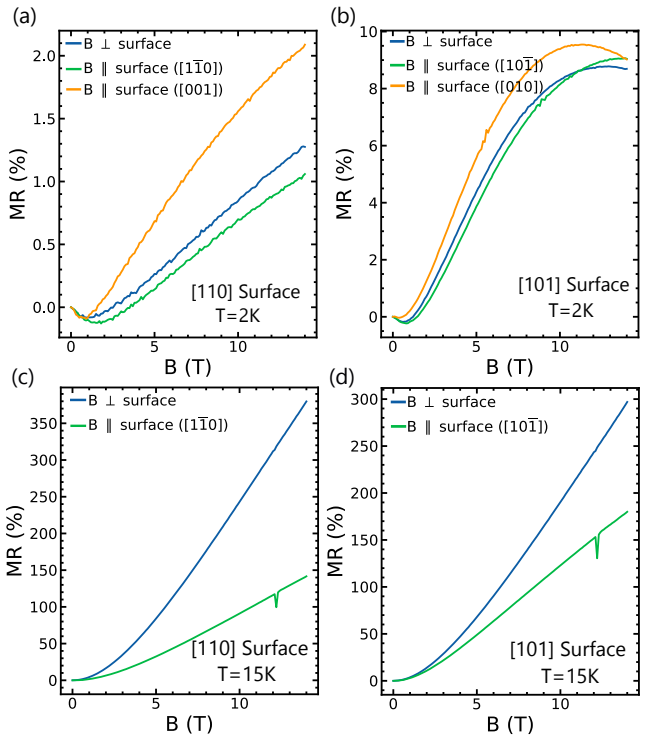

FIG. 2. In-plane and out-of-plane field sweeps for (a-b) the surface dominated transport regime and (c-d) the bulk dominated transport regime.

Determining the power law of variable-range hopping conduction

In doped semiconductors near the insulator-to-metal transition, in which overlap between localized states near the Fermi level is the mode of electronic conduction, the logarithmic resistance takes on a universal sub-linear scaling with inverse temperature with a power law that depends on dimensionality, with the exception of hopping within a Coulombic gap:

$$R(T) = \begin{cases} R_0 \exp\left(\frac{\varepsilon}{k_B T}\right) & \text{Nearest-neighbor hopping} \\ R_1 \exp\left(\left(\frac{\varepsilon}{k_B T}\right)^{\frac{1}{d+1}}\right) & \text{VRH (Uncorrelated)} \\ R_2 \exp\left(\left(\frac{\varepsilon}{k_B T}\right)^{\frac{1}{2}}\right) & \text{VRH (Coulomb gap)} \end{cases} \quad (2)$$

With some exceptions to this universal scaling, even within the same chemical system with variations in doping level (e.g. p-type Ge) Zabrodskii proposed a method of determining more reliably the power law associated with the hopping regime by using the logarithmic derivative of resistance with temperature:

$$W = \left(\frac{\varepsilon}{k_B T}\right)^x = -\frac{d\log(\rho)}{d\log(T)} \quad (3)$$

and plotting this value on a log-log plot with temperature to find the power law via the slope of this plot [1]. We plot this quantity for the low temperature conduction on the [110] and [101] surface of $FeSb_2$ in figure 3. Results from comparing the slope of these plots with expectation for Coulombic, 2D, and 3D variable range hopping power laws show best agreement with 3D variable range hopping.

In addition to the Zabrodskii technique, we include a comparison of 2D and 3D power law fits and their respective residuals in figure 4 from the fits to show that the 3D VRH scaling fits give a temperature independent residual over much of the temperature range fit whereas the 2D scaling gives large temperature dependence in the fit residuals showing clear disagreement.

On the reports of 2D VRH power law in SmB_6

Recent reports of low temperature transport in SmB_6 samples grown by floating zone presents evidence of 2D variable range hopping conduction [2], The authors claim that they do not find agreement with 3D VRH scaling, but do not provide evidence of fits or attempts to find an appropriate scaling law. Instead, a two-channel model is used in which there is a 2D VRH channel in parallel with a temperature independent conductivity of the form

$$R(T)^{-1} = R_n^{-1} + R_{2D}^{-1} \exp\left(-\left(\frac{T_{VRH}}{T}\right)^{1/3}\right) \quad (4)$$

where R_n is the channel resistance for the temperature independent channel in parallel with the hopping conduction channel, which is determined from fit.

In figure 5, we compare data from this paper with a single-channel 3D VRH conduction scalling and find good agreement, supporting the ubiquity of this hopping scaling across localized surface states in $FeSb_2$, Te-flux grown FeSi and now floating zone grown SmB_6.

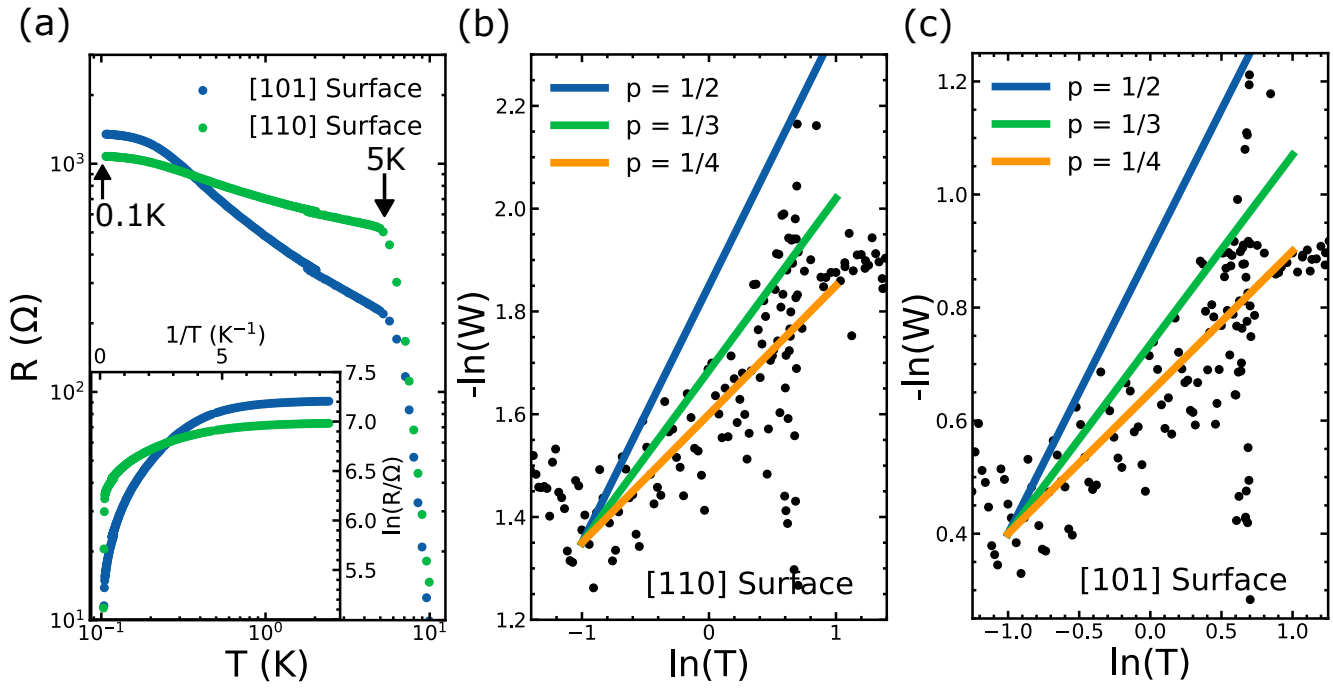

FIG. 3. Zabrodskii plots to determine the power law of variable range hopping conduction at low temperatures for (b) $FeSb_2$ [110] surface and (c) $FeSb_2$ [101] surface.

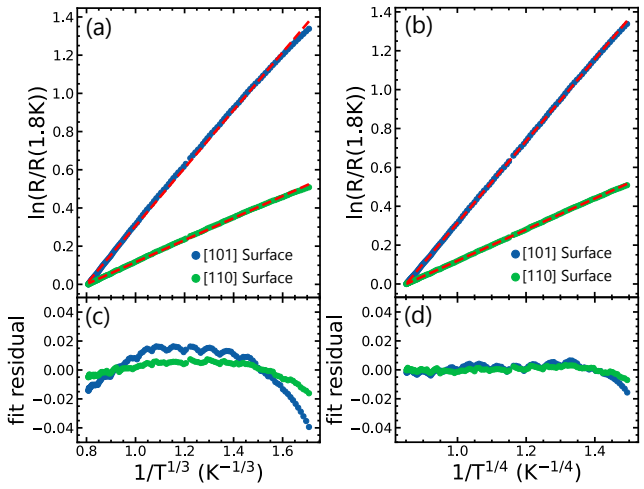

FIG. 4. Comparison of fits of $FeSb_2$ VRH data to 2D (a) and 3D (b) variable range hopping scaling laws and their respective fit residuals (c-d).

[1] A. G. Zabrodskii, Philosophical Magazine B **81**, 1131–1151 (2001).

[2] M. Batkova, I. Batko, S. Gabáni, E. Gažo, E. Konovalova, and V. Filippov, Physica B: Condensed Matter **536**, 200–202 (2018).

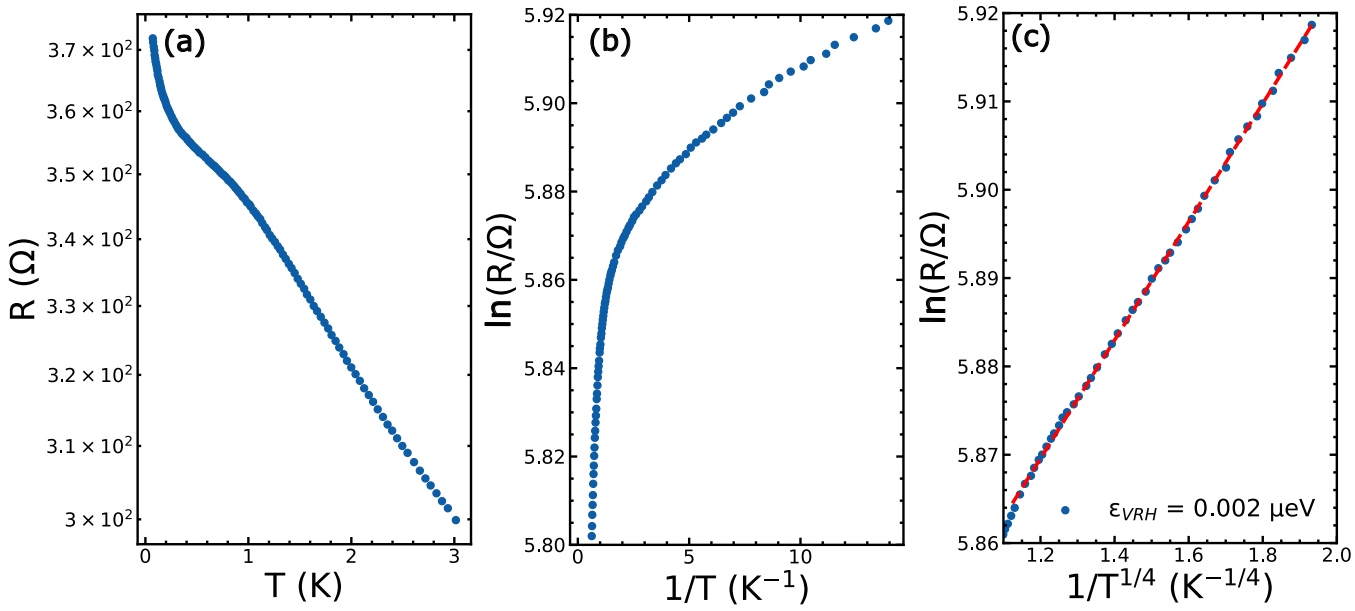

FIG. 5. Data digitized from reference [2] on the low temperature transport in SmB_6 showing agreement with $T^{1/4}$ power law.